# Sonochemical Synthesis of Nanocrystalline Rare Earth Orthoferrites Using $Fe(CO)_5$ Precursor

M. Sivakumar,[†] A. Gedanken,*[,†] D. Bhattacharya,[§,⊥] I. Brukental,[§] Y. Yeshurun,[§] W. Zhong,[‡] Y. W. Du,[‡] I. Felner,[∥] and I. Nowik[∥]

*Department of Chemistry, Bar-Ilan University, Ramat-Gan 52900, Israel, National Laboratory of Solid State Microstructures, Nanjing University, Nanjing 210093, P. R. China, Department of Physics, Institute of Superconductivity, Bar-Ilan University, Ramat-Gan 52900 Israel, and The Racah Institute of Physics, The Hebrew University, Jerusalem 91904, Israel*

*Received April 22, 2004. Revised Manuscript Received July 18, 2004*

This paper describes, for the first time, a simple sonochemical method for the synthesis of nanoparticles of a series of rare earth orthoferrites. This sonochemical process is enabling synthesis of nanoparticles of the rare earth orthoferrites at a substantially lower calcination temperature by using simple precursors, iron pentacarbonyl and rare earth carbonates. It is particularly noteworthy that the cogeneration of the garnet phase has not been observed, as is usual with the conventional methods. The drastic reduction in the calcination temperature could be due to the ultrasonic generation of amorphous iron oxide from $Fe(CO)_5$. Nanosized $GdFeO_3$, $ErFeO_3$, $TbFeO_3$, and $EuFeO_3$ were prepared by this method and their magnetic properties were also studied in detail.

## Introduction

Submicroscopic or nanocrystalline materials research is rapidly advancing and thus has attracted the interest of many scientists and engineers due to the unique and fruitful properties conferred by the particles of very small dimensions (<100 nm), in contrast to the corresponding bulk materials.[1,2] This is mainly due to the fact that such materials hold the promise of new technological applications and thus it is apparent that their development continues to grow at a rapid pace in this nanotechnological world.

The class of orthoferrites shows a strong uniaxial anisotropy and was among the first bubble-domain materials discovered in the 1960s. Backed by a string of accomplishments, at the heart of nanofield, the successful preparation of nanosized ferrites with precise stoichiometry poses a synthetic challenge, particularly in the case of complex materials containing two or more metallic elements.[3−5] The most prominent methods that have been reported like solid-state powder synthesis or melting procedures, based on extensive mechanical grinding of the corresponding oxides, i.e., $Ln_2O_3$ (Ln = any lanthanide element) and $Fe_2O_3$ in order to ensure homogeneous mixing along with subjecting at a high enough calcination temperature (∼1800 °C in the formation of $GdFeO_3$).[6] These rigorous conditions lead to bulk materials, which may or may not exhibit a nanocrystalline structure. In addition, the process involving a higher calcination temperature has several problems, e.g., poor homogeneity, high porosity, and poor control of the particle size, which indirectly affects the functional properties of the obtained powders.

Traditional wet chemistry approaches to synthesize $LnFeO_3$ are based on preparing a precursor solution, which contains the sources of $Ln^{3+}$ and $Fe^{3+}$. Since no positional control is offered, the rare earth ion and the iron compounds present in the reaction mixture randomly collide to form various intermediate species with metal ratios unfavorable for obtaining a single-phase material. The result is the coexistence of the undesired phases, e.g., $Ln_3Fe_5O_{12}$ and $Fe_3O_4$, in the final ceramic material.[6] Thus, phase-selective synthesis of $LnFeO_3$ oxides poses problems as the process favors the thermodynamically more stable magnetic garnets ($Ln_3Fe_5O_{12}$). All of the above facts suggest that obtaining nanosized single-phase orthoferrite powders have therefore been difficult and alternate technologies or newer processing techniques are thus required, to address and overcome the constraints inherent with the conventional methods.

Motivated by the above needs, this paper investigates the synthesis of rare earth orthoferrites using a novel sonochemical method for the first time. Sonochemistry offers a quick and facile method to generate novel

* To whom correspondence should be addressed. E-mail: gedanken@mail.biu.ac.il. Fax: 972-3-5351250.
† Department of Chemistry, Bar-Ilan University.
‡ Nanjing University.
§ Department of Physics, Bar-Ilan University.
∥ The Hebrew University.
⊥ Present address: Electroceramics Division, Central Glass and Ceramic Research Institute, Calcutta 700 032, India.

(1) Lau, M. L.; Jiang, H. G.; Perez, R. J.; Juarezislas, J.; Lavernia, E. J. *Nanostruct. Mater.* **1996**, *7*, 847.
(2) Minh, N. Q. *J. Am. Ceram. Soc.* **1993**, *76*, 563.
(3) Zheng, W. J.; Liu, R. H.; Peng, D. K.; Meng, G. Y. *Mater. Lett.* **2000**, *43*, 19.
(4) Manoharan, S. S.; Patil, K. C. *J. Solid State Chem.* **1993**, *102*, 267.
(5) Chakraborty, A.; Devi, P. S.; Maiti, H. S. *J. Mater. Res.* **1995**, *10*, 918.
(6) Mathur, S.; Shen H.; Lecerf, N.; Kjekshus, A.; Fjellvag, H.; Goya, G. F. *Adv. Mater.* **2002**, *14*, 1405.

10.1021/cm049345x CCC: $27.50 
Published on Web 08/27/2004

materials with unprecedented technological potential and thus it is not surprising to see its increasingly important role and unparalleled opportunities it offers to generate novel materials.[7] Sonochemistry refers to processes in which passing ultrasonic waves induces chemical changes. This powerful tool utilizes ultrasound and generates cavitation in a liquid in which it passes. Cavitation is the generation, growth, and implosive collapse of the bubbles, which results in intense collapse conditions, locally but at millions of locations. These intense conditions generated are responsible for unique materials obtained in this process.[8] The main advantage of this method is achieving the product formed, which is made up of fine particles of nanometer dimension.

In addition to that, the calcination temperature applied in the current preparation of the rare earth orthoferrites is also very low (800−910 °C), and to the best of our knowledge, this is the lowest calcination temperature that has been applied in the formation of a single phase of orthoferrites.

## Experimental Section

**Materials.** The starting materials used in the present work included gadolinium(III) nitrate hexahydrate (Aldrich, 99.99%), erbium(III) nitrate pentahydrate (Aldrich, 99.9%), europium(III) nitrate pentahydrate (Aldrich, 99.9%), terbium(III) nitrate pentahydrate (Aldrich, 99.9%), urea (Aldrich, 98%), $Fe(CO)_5$ (Strem chemicals, USA, 99.5%), Decalin (Acros organics, 98%), and pentane (96%, Bio-lab, Israel).

**Characterization.** The phase constitution of the obtained products was characterized by employing a Rigaku X-ray diffractometer (Model-2028, Co Kα radiation). XRD measurements were taken in the $2\theta$ scanning range from 15° to 70°. The microstructures of the products were determined by transmission electron microscopy (TEM) (JEOL-JEM 100SX microscope). Samples for TEM were prepared by dispersing them in alcohol using ultrasound and placing a drop of this solution on an amorphous carbon film on copper grid (400 mesh, Electron Microscopy Sciences) and allowing them to dry in air. FT-IR spectra were recorded on a Nicolet (Impact 410) infrared spectrophotometer with KBr pellets over a 400−4000 $cm^{-1}$ range. Energy-dispersive X-ray analysis (EDS) was carried out on a JEOL-JSM-840 scanning microscope. Complex permeability spectra were measured with a coaxial transmission line connected to an impedance analyzer (Agilent4284A from 20 Hz to 1 MHz), or an impedance/material analyzer (Agilent4191B from 1 MHz to 1.8 GHz). The magnetization vs temperature, as well as hysteresis loops at different temperatures, within the temperature range 5−300 K, were measured in a SQUID magnetometer coupled with a superconducting magnet (MPMS-5S, Quantum Design).

**Preparation Procedures.** The present sonochemical method makes use of ultrasound irradiation in two stages: (i) synthesizing rare earth carbonates and (ii) decomposing $Fe(CO)_5$ and dispersing the in situ formed amorphous $Fe_2O_3$ onto the prepared rare earth carbonates obtained in the first stage to obtain the precursor. Calcination of this precursor then results in the formation of a fine ferrite powder.

**Stage 1: Preparation of Rare Earth Carbonates.** The synthesis of rare earth carbonate particles was carried out with the aid of ultrasound radiation. In a typical synthetic process, 5 g of urea was added to an aqueous solution (50 mL) of 1.0 g of the respective rare earth nitrate in a sonication flask. The resultant solution was then irradiated for 3 h with high-intensity ultrasound radiation by employing a direct immersion titanium horn (Sonics and Materials, 20 kHz, 600 W). Calorimetry was used to estimate the electro-acoustic or energy transfer efficiency of the transducer to the solution. Based on the calorimetry experiments, the transfer efficiency of the ultrasonic energy from the transducer to the reactor solution was estimated as 54% (at 65% amplitude), with the assumption that all the ultrasonic energy was converted to heat in the reactor. Based on these calorimetry measurements, the power intensity of the system was calculated as 29.7 $W/cm^2$. The titanium horn tip was inserted into the solution to a depth of 1 cm. The temperature during the experiment increased to a maximum of 85 °C due to ultrasound passage, as measured by an iron constantan thermocouple. After 3 h of reaction, it was then cooled to room temperature. The obtained white solid product was then separated from the solution by centrifugation. After centrifugation, the recovered product was washed with doubly distilled water and ethanol several times and dried under vacuum at room temperature. The obtained vacuum-dried rare earth carbonates were used in the second stage.

**Stage 2: Preparation of Amorphous $Fe_2O_3$ from $Fe(CO)_5$ and in Situ Dispersion of the Obtained Product on Rare Earth Carbonates.** This step utilizes the principle of obtaining pure amorphous materials from suitable precursors by means of sonication.[9,10] Suslick and co-workers have already prepared pure amorphous iron,[9] amorphous cobalt, amorphous Fe/Co alloy,[11] and amorphous molybdenum carbide,[12] using ultrasound. Following the same principle, the present approach involves generating amorphous $Fe_2O_3$ from iron pentacarbonyl by ultrasound, after which the resultant amorphous $Fe_2O_3$ generated was dispersed in situ on the respective rare earth carbonates, again with the assistance of ultrasound. The process involves taking stoichiometric amounts of rare earth carbonates and $Fe(CO)_5$ in Decalin and irradiating with ultrasound. The reaction was carried out in an atmosphere of air at a temperature of 0 °C for 4 h, after which the obtained product was thoroughly washed with pentane, centrifuged, and dried in a vacuum at room temperature. The product thus obtained will hereafter be referred to as the precursor. The precursors obtained were then calcined between 800 and 910 °C for 24 h in an air atmosphere to obtain the corresponding nano-orthoferrite fine powder.

## Results and Discussion

**(A) XRD.** From the literature it can be seen that in order to obtain pure and well-crystallized orthoferrites, it is necessary to subject the materials for calcination at high enough temperature of 1800 °C.[6] For shorter periods of time as well as reduced calcination temperatures, X-ray patterns still show peaks of the corresponding rare earth oxides and α-$Fe_2O_3$ that have not reacted. But in the present sonochemical method it has been observed that all the orthoferrites crystallize at temperatures as low as in the range between 800 and 910 °C. Figure 1 shows the XRD patterns of the obtained orthoferrites which show a high degree of crystallinity indicated by the appearance of the most intense reflections. The diffraction peaks of these ferrites match those reported for the standard.

(7) Suslick, K. S., Ed. *Ultrasound: Its chemical, physical and biological effects*; VCH Publishers: New York, 1988.

(8) Suslick, K. S.; Fang, M.; Hyeon, T.; Cichowlas, A. A. In *Molecularly Designed Ultrafine Nanostructured Materials*; Gonsalves, K. E., Chow, G. M., Xiao, T. O., Cammarata, R. C., Eds.; MRS Symposium Proceedings 351; Materials Research Society: Pittsburgh, PA, 1994.

(9) Suslick, K. S.; Choe, S. B.; Cichowlas, A. A.; Grinstaff, M. W. *Nature* **1991**, *353*, 414.

(10) Cao, X.; Koltypin, Y.; Prozorov, R.; Kataby, G.; Gedanken, A. *J. Mater. Chem.* **1997**, *7*, 2447.

(11) Bellissent, R.; Galli, G.; Hyeon, T.; Magazu, S.; Majolino, D.; Migliardo, P.; Suslick, K. S. *Phys. Scr.* **1995**, *T57*, 79.

(12) Hyeon, T. H.; Fang, M. M.; Suslick, K. S. *J. Am. Chem. Soc.* **1996**, *118*, 5492.

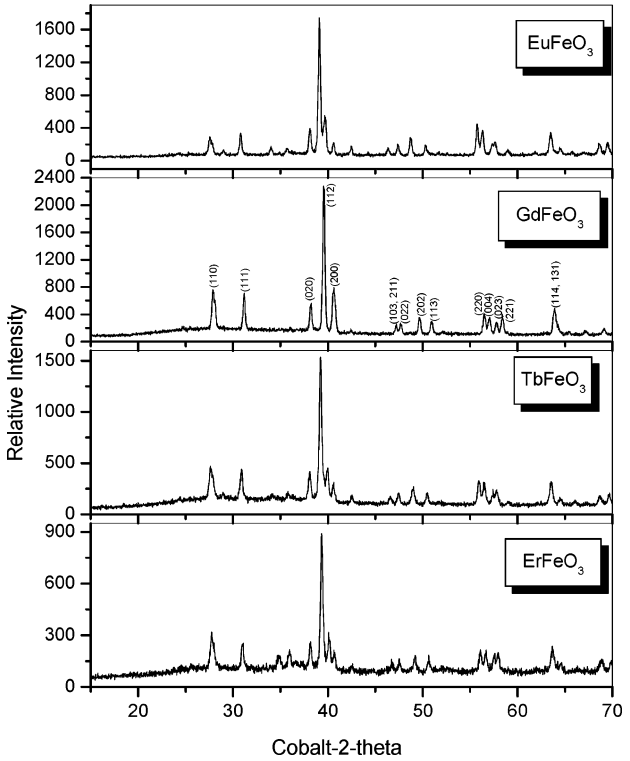


**Figure 1.** Powder X-ray diffraction patterns of the obtained orthoferrites: $EuFeO_3$, $GdFeO_3$, $TbFeO_3$, and $ErFeO_3$.

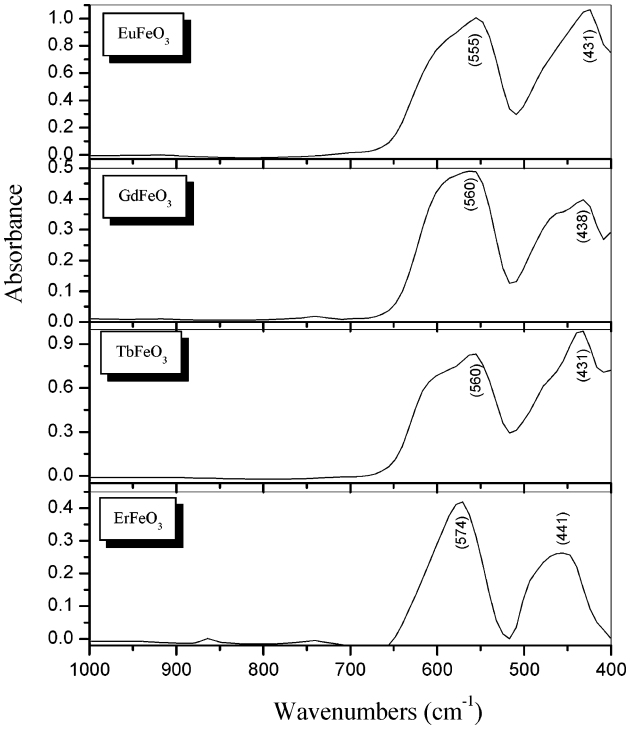


**Figure 2.** IR spectra of the obtained orthoferrites: $EuFeO_3$, $GdFeO_3$, $TbFeO_3$, and $ErFeO_3$.

**(B) IR.** Further evidence for the formation of these orthoferrites comes from IR. The IR spectra of these nanocrystalline ferrites in the frequency range from 1000 to 400 $cm^{-1}$ have been shown in Figure 2. The spectrum of each ferrite shows well-established strong absorption bands around ~560 and ~440 $cm^{-1}$. The existence of a band around 560 $cm^{-1}$ strongly suggests the Fe−O stretching vibration ($\gamma_1$ mode), and the

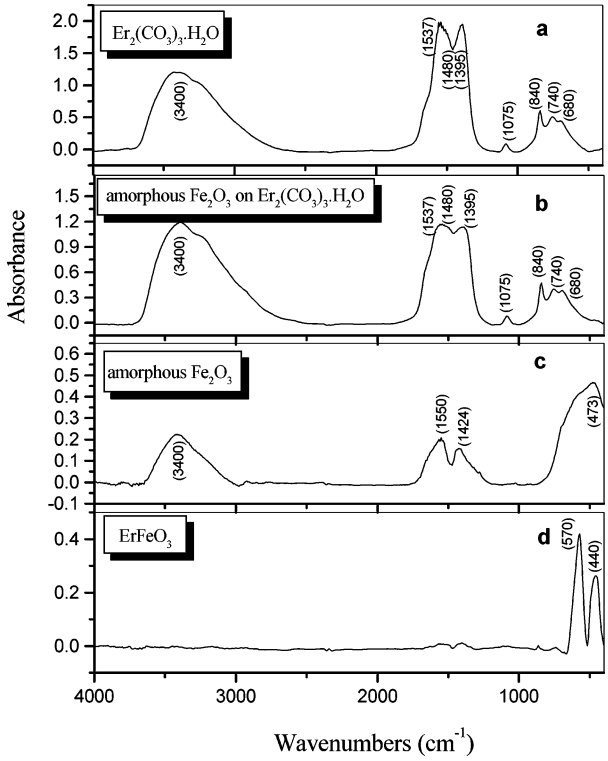


**Figure 3.** IR spectra of the (a) as-synthesized $Er_2(CO_3)_3 \cdot H_2O$, (b) amorphous $Fe_2O_3$ dispersed on $Er_2(CO_3)_3 \cdot H_2O$, (c) amorphous $Fe_2O_3$ (for comparison), and (d) $ErFeO_3$.

440 $cm^{-1}$ band corresponds to the O−Fe−O deformation vibration ($\gamma_2$ mode).[13]

Furthermore, to provide concrete evidence for the formation of pure ferrite phase from the precursor, comparison of IR spectra of the products for one of the ferrites has been shown in Figure 3. It shows the IR spectra of the erbium carbonate, amorphous iron oxide dispersed on erbium carbonate, amorphous iron oxide (for comparison), and calcinated nanocrystalline $ErFeO_3$ powder obtained in the frequency range from 4000 to 400 $cm^{-1}$. The IR spectra of Figures 3a and 3b provide evidence for the presence of carbonate ions in $Er_2(CO_3)_3 \cdot H_2O$ and in the precursor, respectively. In addition, they also show a broad band at ca. 3400, which can be attributed to the stretching mode of hydroxyl groups of bound water molecules. Also, a band at ca. 1395 $cm^{-1}$ observed is assigned to the bending vibrational mode of bound water molecules. In addition, the absorption band at ca. 1480 $cm^{-1}$ had been attributed to the $\gamma_3$ mode of the $CO_3^{2-}$ ion. The other bands at ca. 1075, 840, and 740 $cm^{-1}$ had been assigned to the $\gamma_1$, $\gamma_2$, and $\gamma_4$ modes of the carbonate ions, respectively.[13] Figure 3b shows a spectrum similar to that of Figure 3a, except that its intensities are less, probably due to the presence of amorphous $Fe_2O_3$. The IR spectrum of the amorphous $Fe_2O_3$ synthesized by ultrasound alone (for comparison) shows absorption bands at 473, 1424, and 1550 $cm^{-1}$ in Figure 3c. Figure 3d shows the IR spectrum of $ErFeO_3$. In a comparison of Figure 3d with Figure 3b, we can see after calcination the characteristic bands of $Er_2(CO_3)_3 \cdot H_2O$ and amorphous iron oxide vanish at this calcination temperature and only Fe−O stretching

(13) Rao, G. V. S.; Rao, C. N. R.; Ferraro, J. R. *Appl. Spectrosc.* **1970**, *24*, 436.

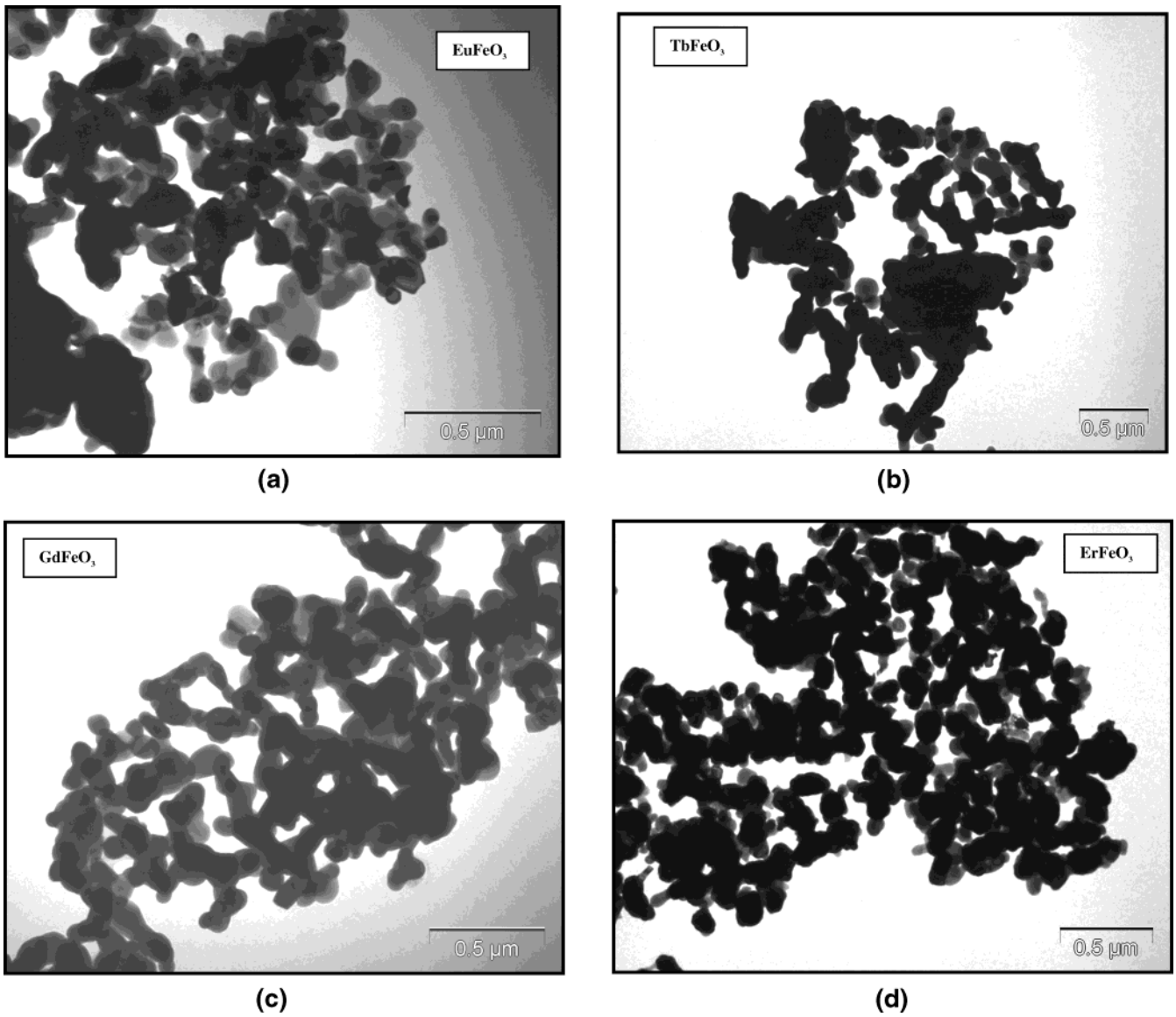


**Figure 4.** Representative conventional transmission electron images of the synthesized orthoferrites (a) $EuFeO_3$, (b) $GdFeO_3$, (c) $TbFeO_3$, and (d) $ErFeO_3$.

vibration bands exist in the synthesized powder. The above interpretation of the IR spectral results is based on the assumption that the synthesized carbonate, $Fe_2O_3$, precursor, and erbium ferrite are essentially pure materials. These results agree with the XRD phase-analysis findings.

**(C) EDS.** The elemental analysis using EDS indicates that all the ferrite products have the Ln:Fe ratio to be 1:1 (within the range of 0.98−1.01), indicating the presence of Ln and Fe in the sample (where Ln = Gd, Er, Tb, and Eu).

**(D) TEM.** Figure 4 shows the representative TEM images of the synthesized orthoferrites using ultrasound. It could easily be observed from these micrographs that, after calcination, the particles have an average diameter of about 60 nm in cases of $GdFeO_3$ and $TbFeO_3$ and 40 nm in cases of $ErFeO_3$ and $EuFeO_3$. This additional evidence confirms that these small particles obtained by this sonochemical method are indeed nanometer in dimension. No remaining corresponding carbonates and $Fe_2O_3$ could be observed in the micrographs despite the low heat treatment temperature. (This could be confirmed by comparing the TEM images of the corresponding rare earth carbonates, amorphous $Fe_2O_3$ dispersed on the rare earth carbonates and the ferrites). This result agrees with the results of XRD and IR.

**(E) Magnetic Properties of the Nanoparticle Rare Earth Orthoferrite Systems.** The "puckered" perovskite rare earth orthoferrites $RFeO_3$ are an important class of materials as they depict antiferroelectric or ferrielectric as well as antiferromagnetic or weakly ferromagnetic behaviors across different temperature regimes. Detailed studies carried out during the 1960s and 1970s and in recent times have revealed many important features of the magnetic properties of these orthoferrites. For instance, in bulk systems, one observes the following: (i) G-type antiferromagnetic spin order below a characteristic Neel temperature $T_N$ across $Fe^{3+}-O^{2-}-Fe^{3+}$ bonds due to superexchange interaction;[14] (ii) $T_N$ varies with the $Fe^{3+}-O^{2-}-Fe^{3+}$ bond angle

(14) Nikolov, O.; Hall, I.; Barilo, S. N.; Mukhin, A. A. *J. Magn. Magn. Mater.* **1996**, *152*, 75.

($\theta$), and with the drop in $\theta$, as a result of replacement of the R-site ion from "La" to "Lu", $T_N$ drops from ~700 to ~600 K;[15] (iii) the magnetic lattice is comprised of collinear antiferromagnetic spin order along a particular crystallographic direction and a canted spin order (which gives rise to weak ferromagnetism), as a result of antisymmetric exchange (*Dzyaloshinskii*-Moriya) coupling,[16] along another crystallographic direction; (iv) the canting angle α varies between 0.5° and 1.5° and increases as the R-site ion is changed from "La" to "Lu";[15] (v) the internal field $H_{in}$, related to the Fe sublattice magnetism and, in turn, to the exchange coupling $|J|$, varies with temperature and increases from "$LaFeO_3$" to "$LuFeO_3$" ion;[15] (vi) a spin reorientation takes place with swapping of antiferromagnetic and ferromagnetic spin order direction at lower temperature and under a high magnetic field; (vii) the "R" sublattice develops a magnetic order at low temperature (<10 K); interaction between "Fe" and "R" sublattices leads to the spin reorientation; the spin reorientation is found to be a continuous process.[17]

Such a set of rich features of the orthoferrites, though, attracted the attention of researchers yet the *antiferromagnetic* and weak ferromagnetic properties prevent them from being used widely. The "soft" and "hard" ferrites having spinel structure, on the other hand, exhibit *ferromagnetic* properties suitable for many applications. The nanoparticles of such systems exhibit "superparamagnetism" above the blocking temperature ($T_B$).[18] The nanoparticles of the *antiferromagnetic* systems essentially develop a bilayer core−shell structure with core lattice and surface having uncompensated spins. As such, this system offers a better option for studying magnetic quantum tunneling phenomenon as opposed to nanoparticle ferromagnetic systems.[19]

Given such a background, it would be interesting to explore the magnetic properties of the nanoparticle orthoferrite systems to find out whether nanosystems offer qualitatively superior property and/or maneuverability. The reports in the published literature, in this regard, are scanty.[6] Therefore, the purpose of our work was to explore the magnetic properties of nanoparticles of a series of rare earth orthoferrite systems. In this paper, we report the results obtained from our systematic global magnetic study of the nanoparticle orthoferrite systems. We observe certain interesting features in the variation of key magnetic properties like transition temperatures, magnetization, coercivity, etc. as the R-site ion changed from "La" to "Er".

In the following, we present and discuss the results of the magnetic properties measurements carried out on nanoparticle $LaFeO_3$, $EuFeO_3$, $GdFeO_3$, $TbFeO_3$, and $ErFeO_3$ systems synthesized by the present sonochemical method. Synthesis of lanthanum ferrite nanoparticles by the sonochemical method has already been reported by our group.[20]

In Figure 5a, we show the variation of magnetic moment with temperature measured over 5−300 K. The following features are evident here: (i) None of the systems depict a cusp in the pattern, expected in superparamagnetic antiferromagnetic systems, within the temperature range studied; the cusp, in fact, signals deviation from superparamagnetic behavior at lower temperature;[21] this could be because of the multidomain nature and larger size of the particles in our samples in comparison to the single domain size (Figure 4). (ii) Clear antiferromagnetic order sets in at around ~246 K in the $EuFeO_3$ system. (iii) In the case of the $LaFeO_3$ system too, deviation from Curie−Weiss paramagnetism is evident within the temperature regime 5−300 K as magnetic order across Fe−O−Fe bonds sets in at even higher temperature and there is no paramagnetic contribution from $La^{3+}$. (iv) In all other systems, of course, no clear magnetic transition is evident, even though, at lower temperature (<50 K), one does observe the deviation from the Curie−Weiss pattern which could be because of the onset of short-range interaction among the $R^{3+}$ ions, which eventually leads to an order at lower temperature. Fitting of the experimental magnetization vs temperature pattern by Curie−Weiss law $\chi = C/(T - \theta)$ yields the Curie and Weiss constants $C$ and $\theta$. They are found to vary with R-site ion. While $\mu_{eff}$ varies across the range 5.25−8.5 $\mu_B$ ($RFeO_3$ molecule has been considered for calculation) for $LaFeO_3$, $EuFeO_3$, $GdFeO_3$, $TbFeO_3$, and $ErFeO_3$ systems, $\theta$ varies between −40 and −12 K for $ErFeO_3$, $TbFeO_3$, and $GdFeO_3$ systems. $\theta$ shoots up to −550 K in the case of the $EuFeO_3$ system. The Curie−Weiss plots for the relevant systems are shown in Figure 5b. It is to be noted that the paramagnetism in these systems could result either from the superparamagnetic component, if any, and/or from the $R^{3+}$ ion paramagnetic component as magnetic order in the $R^{3+}$ sublattice sets in at a very low temperature (<10 K). The $Fe^{3+}-O^{2-}-Fe^3$ order gives rise to antiferromagnetic and/or weakly ferromagnetic order. *In the absence of superparamagnetism within the given temperature range in our systems, paramagnetism results solely from the contribution of $R^{3+}$ ions*. Of course, in a core−shell type structure, surface magnetism, because of uncompensated spins, can also contribute. The paramagnetic contribution of $R^{3+}$ ions varies from 0.0 to 9.5 $\mu_B$ across "La" to "Er". Comparison of net magnetic moment for the $RFeO_3$ system with the paramagnetic moment contribution of $R^{3+}$ ion shows that the contribution of the Fe sublattice varies from system to system. As mentioned earlier, in the case of the $LaFeO_3$ system, overall magnetization depends sole on Fe sublattice contribution as a result of which we observe large coercivity (~90 Oe) at room temperature and no Curie−Weiss paramagnetism across the temperature range explored here.

For the $EuFeO_3$ system, both the paramagnetic component of $Eu^{3+}$ and the canted antiferromagnetic component of Fe sublattice contributes. Large magne-

(15) Eibschütz, M.; Shtrikman, S.; Treves, D. *Phys. Rev.* **1967**, *156*, 562. Lyubutin, I. S.; Dmitrieva, T. V.; Stepin, A. S. *J. Exp. Theor. Phys.* **1999**, *88*, 590.

(16) Bogdanov, A. N.; Roessler, U. K.; Wolf, M.; Mueller. K. H. cond-mat/0206291, 2002.

(17) Gordetsky, G.; Hornreich, R. M.; Yaeger, I.; Pinto, H.; Shachar, G.; Shaked, H. *Phys. Rev. B* **1973**, *8*, 3398. Pinto, H.; Shachar, G.; Shaked, H.; Shtrikma, S. *Phys. Rev. B* **1971**, *3*, 3861.

(18) Pal, M.; Brahma, P.; Chakravorty, D.; Bhattacharya, D.; Maiti, H. S. *J. Magn. Magn. Mater.* **1996**, *164*, 256.

(19) Lu, R.; Zhang, P. F.; Zhu, J. L.; Chang, L. *Phys. Rev. B* **1997**, *56*, 10993.

(20) Sivakumar, M.; Gedanken, A.; Zhong, W.; Jiang, H. Y.; Du, Y. W.; Brukental, I.; Bhattacharya, D.; Yeshurun, Y.; Nowik, I. *J. Mater. Chem.* **2004**, *14*, 764.

(21) Sorop, T. G.; Evangelisti, M.; Haase, M.; de Jongh, L. J. cond-mat/0304016, 2003.

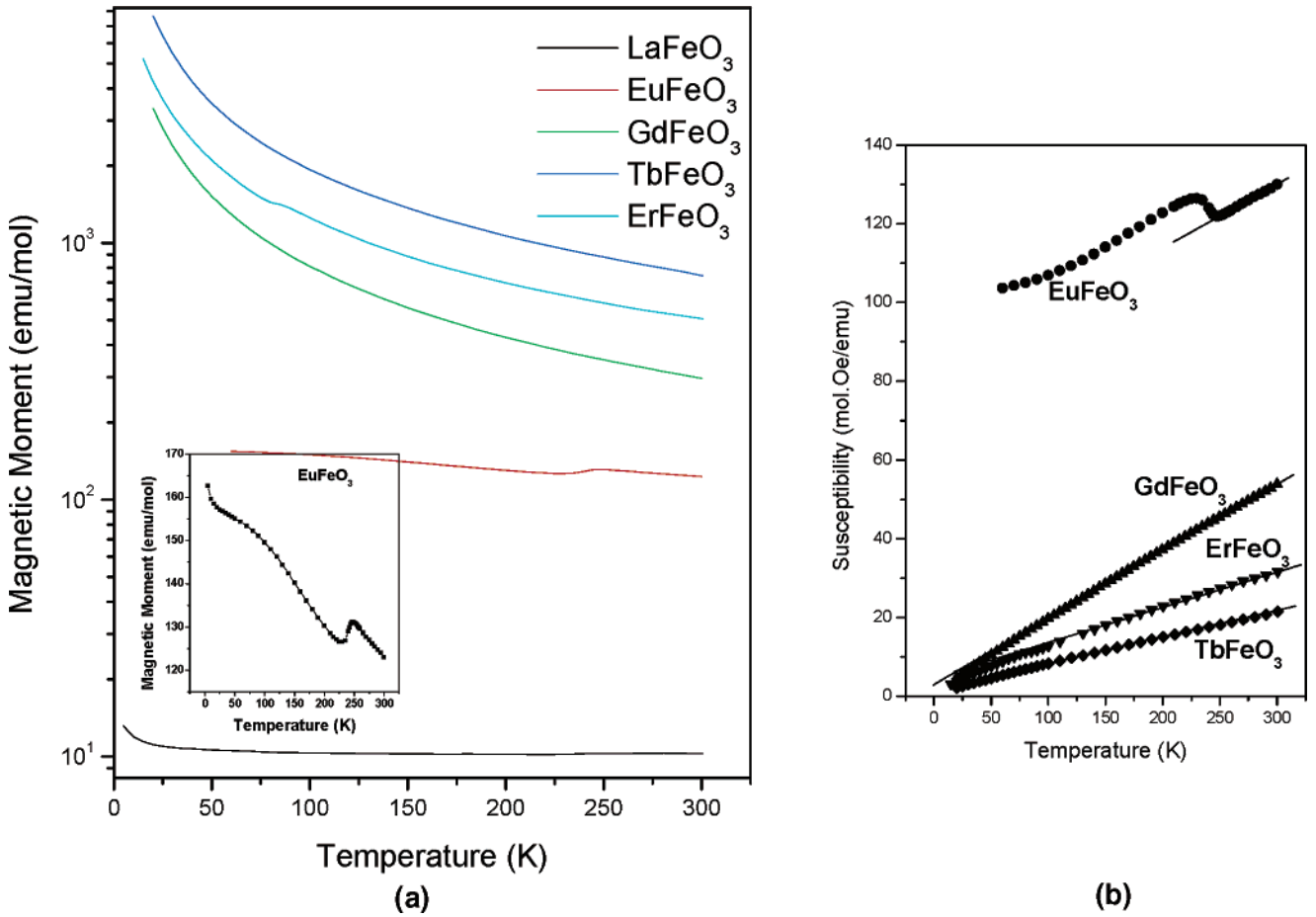


**Figure 5.** (a) Magnetic moment vs temperature for the nanoparticle rare earth orthoferrites. Inset: the pattern for the $EuFeO_3$ system which shows onset of antiferromagnetic order at ~246 K. (b) Curie−Weiss plot (straight line) on susceptibility vs temperature patterns for relevant systems.

tization of the Fe sublattice results in very high coercivity (~700 Oe) at room temperature in this case. On the other hand, the paramagnetic contribution dominates in the $GdFeO_3$ and $TbFeO_3$ systems while in the case of the $ErFeO_3$ system, although one does observe dominance of the paramagnetic component, an order could develop within the $Er^{3+}$ sublattice, which is reflected by its slightly higher $\theta$ (−40 K).

In Figure 6, we show the room temperature hysteresis loops for all the systems. The magnetic moment ($M$) vs field ($H$) pattern is primarily paramagnetic with an exception in the case of $EuFeO_3$. It is evident that the magnetization ($M_s$) at maximum field (~1.6 T) increases systematically as the R-site ion changes from "La" to "Er". This is possibly due to an increase in paramagnetic moment of $R^{3+}$ ion as well as increase in canting angle $\alpha$ in the same order. Interestingly, the $EuFeO_3$ system depicts high coercivity $H_c$ (~700 Oe); in the inset, the hysteresis plot for the $EuFeO_3$ system is blown up. The systems such as $GdFeO_3$, $TbFeO_3$, and $ErFeO_3$ depict smaller coercivity in comparison to that of $EuFeO_3$ at room temperature. The large coercivity in $EuFeO_3$ could well be due to large internal field $H_{in}$ in the system.

We also present here the magnetic hysteresis loops observed at different temperatures in all the systems (Figure 7). The contribution of the Fe sublattice vis-à-vis $R^{3+}$ ions could be observed over the entire temperature and field range. Like the room-temperature patterns (Figure 6), the magnetic moment at high field (~1.6 T) increases in the order "La" to "Tb" at low temperatures too, which is the same as the order of increase in paramagnetic contribution from $R^{3+}$ ions. The anomalous features at low temperature are, however, as follows: (i) in the case of $ErFeO_3$, one observes an anomalous drop in magnetic moment at low temperature, in contrast to the observation made at room temperature (Figure 6), which could be because of the contribution from Er−carbonate present (Figure 3) and/or from $Er^{3+}$−$Er^{3+}$ sublattice; (ii) in the case of $TbFeO_3$, the coercivity ($H_c$) at ~20 K appears to be quite high (~500 Oe).

We now attempt to systematize these observations in light of both fundamental features noted in bulk systems as well as features expected in nanoparticles of antiferromagnetic systems. It has been observed that both the canting angle $\alpha$ and the internal field $H_{in}$ rises as the R-site ion changes from "La" to "Er". The paramagnetic contribution of $R^{3+}$ ion also increases in the same order. All these give rise to higher magnetization $M_s$ at room temperature under a field of ~16 kOe. In the case of $EuFeO_3$, $H_{in}$ jumps high out of the systematic pattern of rise in $H_{in}$ with drop in R-site ion size $r_R$. They seem to have a role to play in the present nanoparticle systems. Although $M_s$ depicts a systematic rise with the drop in ion size $r_R$, the contribution of Fe sublattice (which can be extracted from the hysteresis loop at room temperature by extrapolating the $M(H)$ pattern to $H = 0$) appears to follow an anomalous trend.

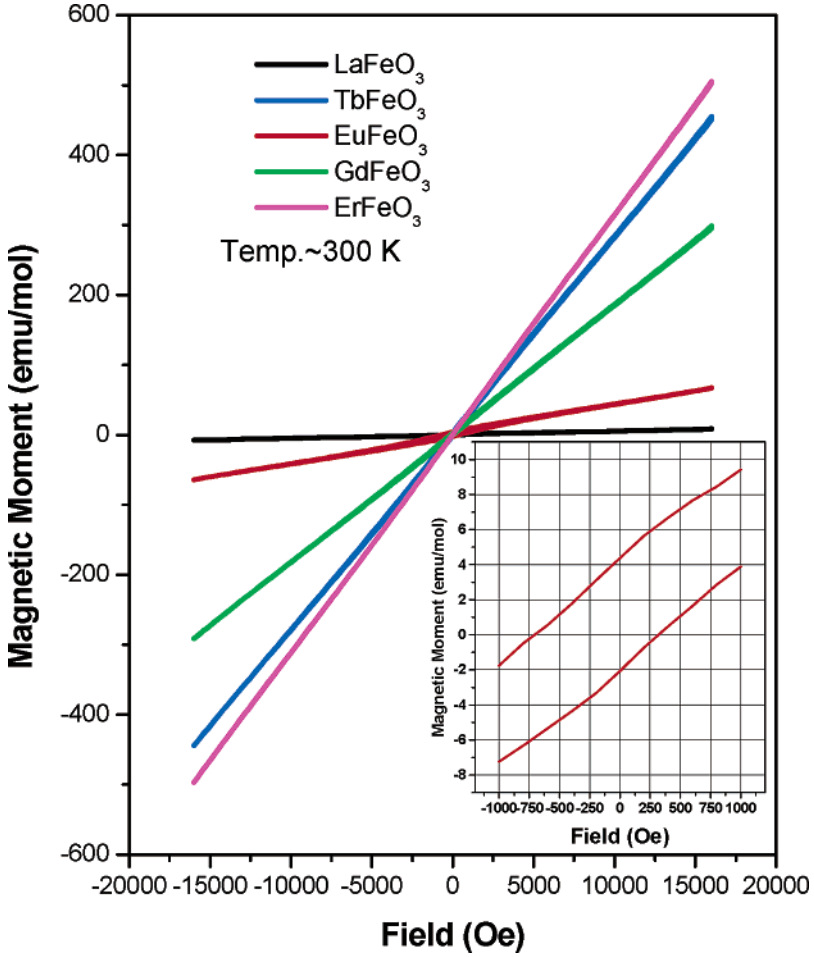


**Figure 6.** Room-temperature hysteresis plots for the nanoparticle rare earth orthoferrite systems; the magnetization at ~1.6 T varies with R-site ion and reaches maximum for the $ErFeO_3$ as the canting angle is maximum for this system.

In the case of the $EuFeO_3$ system, we observe a steep rise in $M$(Fe) which could, once again, be due to the jump in $H_{in}$.

In the case of the $ErFeO_3$ system, on the contrary, we observe a drop in $M$(Fe). One would have expected a systematic rise in $M$(Fe) from "La" to "Er" as the canting angle in the bulk system rises in the same order. We depict the patterns of $M_s$ and $M$(Fe) as a function of tolerance factor $t = (r_R + r_O)/\sqrt{2}(r_{Fe} + r_O)$ in Figure 8. The tolerance factor quantitatively describes the lattice distortion due to variation in $r_R$. Although we used the room-temperature $M_s$ in Figure 8, such relation between $M_s$ and $t$ is valid at lower temperature as well. The reason behind the drop in $M$(Fe) for $ErFeO_3$ is not clear at present.

In summary, we measured the magnetic properties of the nanoparticle orthoferrite systems over a temperature range 5−300 K. In the case of $LaFeO_3$ and $EuFeO_3$ systems, the Fe sublattice seems to be governing the magnetization pattern over a large temperature range. In all other compositions, we observe dominance of the paramagnetic component from $R^{3+}$ ions. The contribution of the Fe sublattice too increases from "La" to "Tb" as canting angle increases in the same order. However, for $EuFeO_3$ one observes a sharp rise in the contribution from Fe sublattice while a drop is seen in the case of the $ErFeO_3$ system. These features contrast the observations made in the bulk systems.

**(F) Permeability Spectra.** A useful route to investigate the mechanism of domain wall motions and domain rotations is to measure the complex permeability as a function of frequency, i.e., the so-called magnetic spectrum. Also, in a study of such a magnetic spectrum, the effective magnetic anisotropy field as well as damping mechanism of domain wall displacements can be checked. In general, the dispersions caused by wall displacements occur in radio frequency range (below 10 MHz), and those caused by domain rotations often appear in the microwave range (100 MHz to10 GHz). Particularly, this methodology has been extensively used in ferrites.[22,23] Thus, a similar study has been carried out in the rare earth orthoferrite samples prepared by the present ultrasonic method.

We have measured the magnetic spectra of the nanoparticle orthoferrite systems at room temperatures. The frequency dependence of real part $\mu'$ and imaginary part $\mu''$ of complex permeability spectra have been shown in Figures 9a and 9b. For permeability measurements, the nanosized powder sample was pressed to a ring with a typical size of 13 mm o.d., 7 mm i.d., and 1 mm thickness. The complex permeability spectra for $TbFeO_3$ have not been measured due to the technical problems (requirement of a large amount of sample).

(22) Rado, G. T.; Wright, R. W.; Emerson, W. H. *Phys. Rev.* **1950**, *80*, 273.
(23) Rado, G. T.; Wright, R. W.; Emerson, W. H.; Terris, A. *Phys. Rev.* **1952**, *88*, 909.

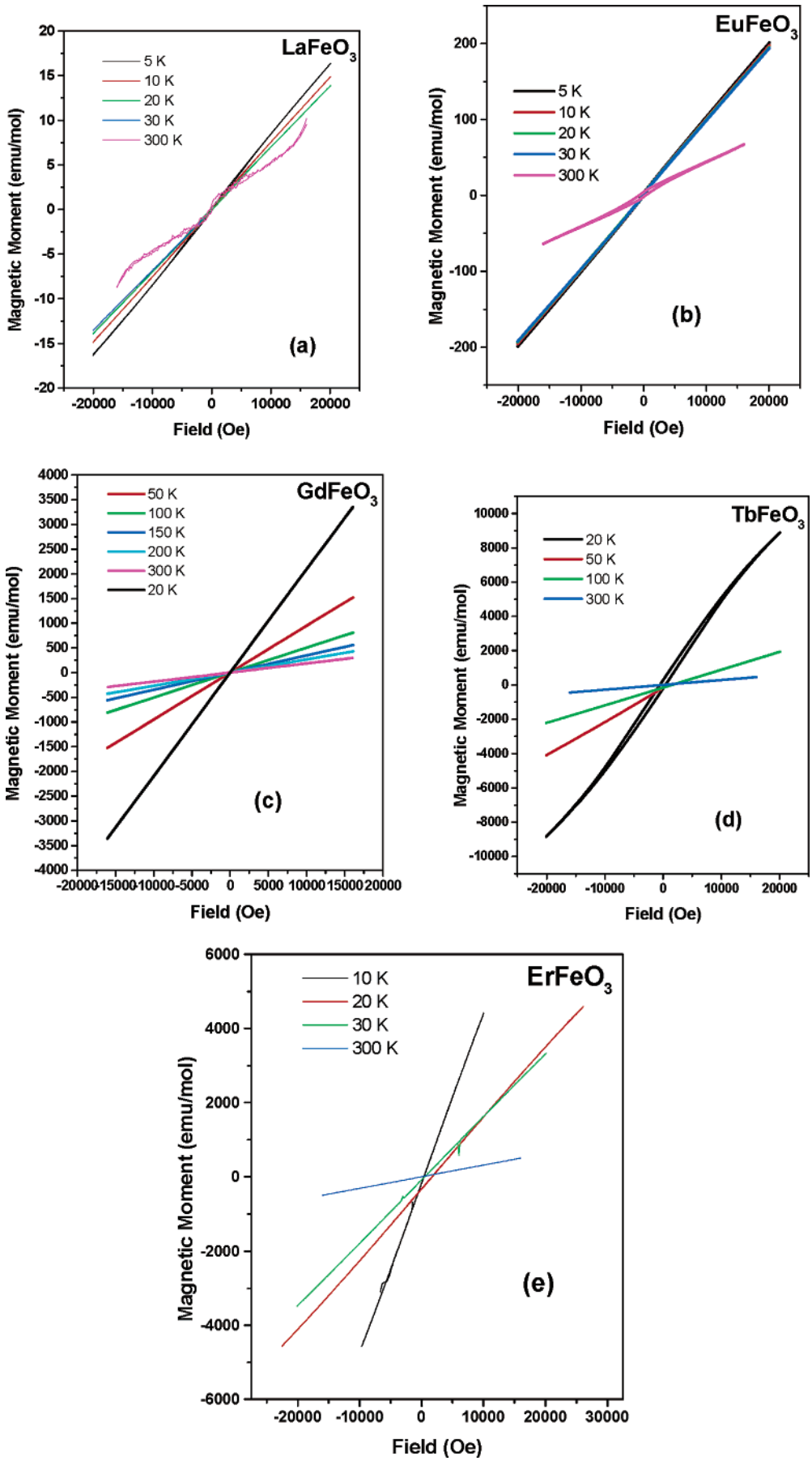


**Figure 7.** Hysteresis plots at different temperatures for the nanoparticle rare earth orthoferrite systems.

One can observe from Figure 9a that for all orthoferrite samples investigated the $\mu'$ value is small and practically constant, at 3−5. According to the theory contemplation, in single domain grains, there are no domain

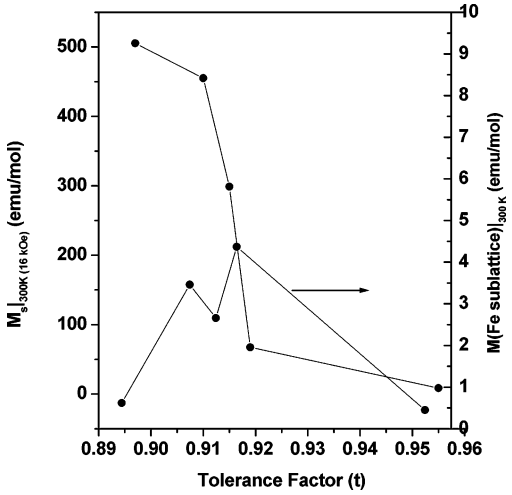


**Figure 8.** Variation of $M_s$ and the contribution of Fe sublattice $M$(Fe) at room temperature with the tolerance factor for the nanoparticle rare earth orthoferrite systems.

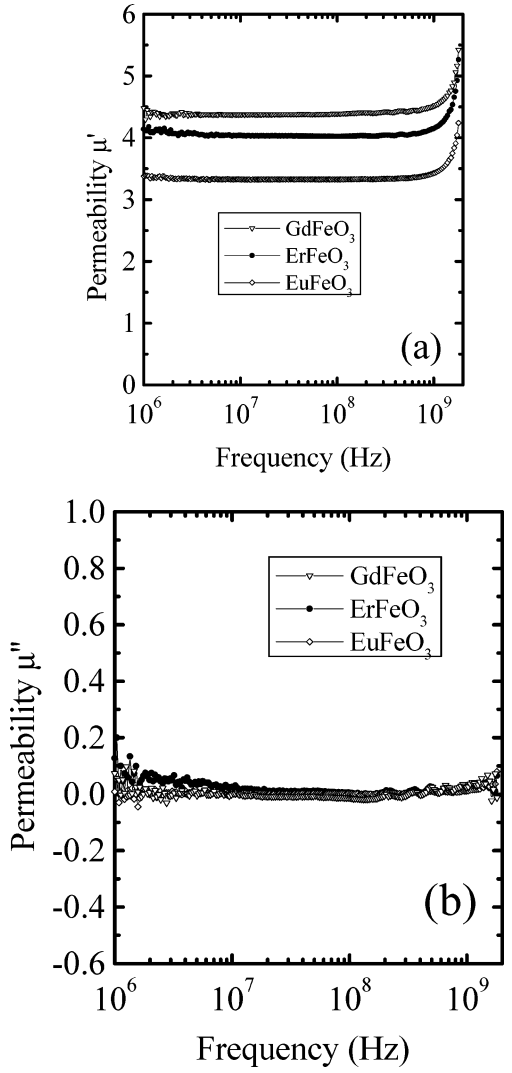


**Figure 9.** The plots of complex permeability: (a) real part $\mu'$ and (b) imaginary part $\mu''$ as a function of frequency for the nanocrystalline rare earth orthoferrite samples at room temperature.

wall motions. Therefore, the $\mu_0$ (static permeability, i.e., $\mu'$ with frequency limit to zero) is only caused by reversible domain rotations and follows the relation $\mu_0 = 1 + 8\pi M_s/3H_a$, where $H_a$ is the effective magnetic anisotropy field. Because the magnetization of the orthoferrite systems at room temperature is very small, the complex permeability is small. The $\mu'$ value measured for the nanoparticle samples is smaller than that of the theory prognosis for corresponding bulk samples. As a result, the pressed ring has lower density than the sintered one. The possible reason could be that the nonmagnetic impurities such as boundaries and cavities from the low density may play an important role and may cause the permeability to decline further. In addition, for the corresponding bulk sample, there is domain wall motion, whereas in nanosized samples, there are only reversible domain rotations. The $\mu_0$ contributed by domain rotations is generally smaller than that by domain wall displacements. The resistivity of the nanoparticle sample is larger than that of the corresponding bulk one, which favors a lower eddy current loss and gives rise to a low value of imaginary part $\mu''$ (shown in Figure 9b).

## Results and Discussion

The role of urea in the homogeneous precipitation of the rare earth carbonate particles (as-synthesized in stage 1) is that it decomposes by hydrolysis homogeneously in the solution upon heating, producing $CO_2$, $OH^-$, and $NH_4^+$ ions in the solution. This increases the pH of the medium, which is suitable for the formation of rare earth carbonate particles. Measurement of the pH before and after the sonication experiment revealed that, depending on the rare earth carbonate, the pH of the solution increased from 5.8 to 6.4. It has been suggested that applying ultrasound radiation during the reaction might accelerate the homogeneous precipitation process. In addition to this, it might also be beneficial in controlling the particle size and the shape.

In the conventional solid-state reaction of $Fe_2O_3$ with rare earth carbonates to form the corresponding orthoferrites $LnFeO_3$, the major limitation is the interaction of molecules or diffusion factor. In the present sonochemical method it is believed that this diffusion resistance may be overcome, as there is an in situ generation of amorphous $Fe_2O_3$ from $Fe(CO)_5$ by ultrasound, followed by its dispersion or deposition on the corresponding rare earth carbonate, and assisted again by ultrasound. This process may have facilitated the diffusion, as well as the reaction, of highly reactive rare earth ion ($Ln^{+3}$) with the amorphous $Fe_2O_3$, consequently resulting in the completion of the phase transition of the precursor to the orthoferrites at a significantly lower calcination temperature employed in the present method.

It appears that the amorphous nature of $Fe_2O_3$ synthesized by ultrasound is another factor which might also play a key role in increasing its reactivity with carbonates, resulting in the formation of a ferrite phase at a lower calcination temperature. The importance of amorphicity in increasing the reactivity has already been addressed.[24] Bellissent et al.[11] have indeed strongly shown that sonochemically prepared amorphous Fe, Co, and Fe−CO nanomaterials are better catalysts than the corresponding crystalline nanomaterials prepared by

(24) Suslick, K. S.; Hyeon, T. W.; Fang, M. M. *Chem. Mater.* **1996**, *8*, 2172.

other methods. In addition, Yee et al.[25] have functionalized amorphous $Fe_2O_3$ nanoparticles with alkanesulfonic and octadecanephosphonic acids. This work further supports the fact that it is possible to form a coating of organic molecules more easily on amorphous $Fe_2O_3$. In addition to the above factors, it is also likely that the size of the reactants (specifically, amorphous $Fe_2O_3$) also contributes to the lowering of calcination temperature.

## Conclusions

In the present investigation, we proposed a sonochemical method and its potential has been demonstrated successfully for the synthesis of rare earth orthoferrites, in the nanometer range, via simple precursors of rare earth carbonates and iron pentacarbonyl, for the first time. This sonochemical method has the distinct advantages of yielding nanocrystalline orthoferrites at a remarkably reduced calcination temperature, showing high reproducibility and obtainment of good morphological homogeneity analogous to a conventional solid-state synthesis. More importantly, no phase segregation or crystallization of other stoichiometries was observed, even at the temperatures of calcination, which confirms the compositional purity of the obtained orthoferrites. An added and striking feature of this technique is that the thermodynamically favored garnet composition, invariably formed in the synthesis of orthoferrites, is not observed using this sonochemical method. These results continue to prove the promising and diversity of applications behind ultrasound-assisted sonochemical processes. Furthermore, these findings are very important because, given the general success of this developed sonochemical approach, it can be anticipated undoubtedly that this method should be able to be used as a prototype reaction for the synthesis of various other ferrites. Taking cognizance of the fact that a particular material may have different magnetic properties depending upon the method of preparation, starting materials, and temperature, ferrites prepared with this method for the above said properties were also investigated in detail.

**Acknowledgment.** Profs. Du and Gedanken thank The Ministries of Science, in China and Israel for a binational grant through the Sino-Israeli program in Materials Science.

CM049345X

(25) Yee, C.; Kataby, G.; Ulman, A.; Prozorov, T.; White, H.; King, A.; Rafailovich, M.; Sokolov, J.; Gedanken, A. *Langmuir* **1999**, *15*, 7111.